

# Migration Pathways as Diagnostic Probes: Benchmarking and Data-Efficient Training of Specialist vs. Generalist Machine-Learned Force Fields

Yi Cao<sup>1</sup> and Paulette Clancy<sup>1\*</sup>

<sup>1\*</sup>Department of Chemical and Biomolecular Engineering, Johns Hopkins University, 3400 N. Charles Street, Baltimore, 21218, Maryland, USA.

\*Corresponding author(s). E-mail(s): [pclancy3@jhu.edu](mailto:pclancy3@jhu.edu);  
Contributing authors: [ycao73@jh.edu](mailto:ycao73@jh.edu);

## Abstract

Machine-learned force fields (MLFFs) are emerging as a cornerstone of computational materials science, enabling simulations at scales inaccessible to first-principles methods. However, a central dilemma persists: should researchers train a bespoke *specialist* potential from scratch, or fine-tune a large *generalist* foundation model for a given material? The trade-offs between data efficiency, predictive robustness, and susceptibility to out-of-distribution failure remain poorly understood. Here, we introduce a generalizable framework that addresses this question by using migration pathways, evaluated via nudged elastic band (NEB) trajectories, as targeted diagnostic probes. Unlike equilibrium-only metrics, migration-based probes test both interpolation and extrapolation performance, providing sharper distinctions between strong and weak models. Using Cr-intercalated  $\text{Sb}_2\text{Te}_3$  as a technologically relevant case study, we benchmark multiple training strategies within the MACE architecture. We show that targeted fine-tuning dramatically improves kinetic property prediction but can induce catastrophic forgetting of long-range physics, producing qualitatively distinct latent representations. Our results highlight migration pathways not only as an efficient benchmark but also as a strategy for generating informative, task-relevant data to guide model improvement. This framework thus bridges benchmarking, data curation, and active learning, offering practical guidelines for developing robust MLFFs across materials classes.

**Keywords:** Machine-learned force fields (MLFFs), Foundation models, Fine-tuning, Migration pathways, 2D materials

# 1 Introduction

The discovery and design of novel two-dimensional (2D) van der Waals materials continues to drive innovation in spintronics, quantum devices, and energy technologies. Among these, topological insulators such as antimony telluride ( $\text{Sb}_2\text{Te}_3$ ) [1, 2] are especially promising, and transition-metal intercalation—for example with chromium (Cr) [3–5]—offers a route to engineer their magnetic and electronic properties. Predicting the stability and dynamics of such doped materials is critical for guiding synthesis and applications. However, the atomic-scale processes that govern functionality—migration, defect diffusion, and interlayer sliding—occur on time and length scales far beyond the reach of density functional theory (DFT) [6–9].

Machine-learned force fields (MLFFs) [10–14] offer a path to overcome this limitation, bringing near-*ab initio* accuracy to molecular dynamics simulations at reduced cost. The advent of large pre-trained “foundation models” such as CHGNet [15], MACE-MP [11], MatterSim [16], and UMA [17] marks a paradigm shift: instead of building narrow, system-specific models, one may transfer broad chemical knowledge to a material of interest through fine-tuning. Yet, the choice between building a *specialist* MLFF from scratch and adapting a *generalist* foundation model remains unresolved. Questions of data efficiency, stability, and transferability—particularly for non-equilibrium processes—are still open.

Existing benchmarks such as Matbench [18] evaluate global accuracy but do not directly probe the kinetic and dynamical processes most relevant to materials applications. Moreover, MLFF failures are often diagnosed post hoc, when molecular dynamics trajectories diverge unphysically, leading to a brute-force cycle of retraining with ever-larger datasets. This is neither efficient nor informative, as it provides little guidance on where and why the model failed.

Here, we propose that migration pathways, evaluated through nudged elastic band (NEB) trajectories, provide a powerful diagnostic probe for MLFFs. Migration-based probes simultaneously challenge interpolation and extrapolation regimes, revealing weaknesses that equilibrium-only tests cannot capture. Beyond benchmarking, these probes also suggest a data-generation strategy: by selectively targeting migration events, one can efficiently expand training sets with the most informative configurations. In this work, we apply this framework to Cr-intercalated  $\text{Sb}_2\text{Te}_3$ , systematically comparing specialist and generalist MLFFs trained under multiple fine-tuning strategies within the MACE architecture. By coupling migration-based probes with latent-space analysis, we not only distinguish strong models from weak ones but also link prediction failures to changes in the learned physical representation.

# 2 Methodology

We employed a systematic approach to benchmark Machine-Learned Force Fields (MLFFs) for Cr-intercalated  $\text{Sb}_2\text{Te}_3$ , comparing specialist models trained from scratch against fine-tuned foundation models.

## 2.1 Data Generation and Model Training

Reference data were generated using Density Functional Theory (DFT) with the PBE functional, comprising 20,000 configurations from ab initio molecular dynamics (AIMD) simulations at multiple temperatures (300K, 600K, 1200K). We employed the MACE architecture for all models due to its state-of-the-art accuracy in representing complex atomic interactions.

Four distinct training strategies were evaluated:

1. **Scratch**: MACE model trained exclusively on our AIMD dataset
2. **Foundation**: Pre-trained MACE-MP model used without fine-tuning
3. **FT-600K**: Foundation model fine-tuned on 5% of data from 600K trajectories
4. **FT-MultiT**: Foundation model fine-tuned on multi-temperature data

## 2.2 Evaluation Framework

Models were assessed through: (i) molecular dynamics simulations at 300K and 600K to evaluate structural stability and transport properties, (ii) nudged elastic band calculations for migration barriers, and (iii) representation learning analysis using t-SNE visualization of physically interpretable descriptors. Performance metrics included force/energy accuracy, dynamic stability, barrier prediction errors, and latent space clustering quality. Detailed computational parameters are provided in Appendix B.

# 3 Results and Discussions

## 3.1 Benchmarking the MLFF Performance in Equilibrium MD Simulations

To make systematic evaluations benchmarking the model performance, we first assessed the performance of each training strategy in molecular dynamics (MD) simulations (Fig. 1a). This provides a comprehensive test of a model’s ability to generate a stable thermodynamic ensemble and accurately reproduce key structural, dynamic, and transport properties. Each model was used to drive a 200 ps simulation, and the resulting trajectories were analyzed as shown in Fig. 1.

All MACE models—foundation, scratch, and fine-tuned variants—successfully reproduce the equilibrium structure of Cr-doped  $\text{Sb}_2\text{Te}_3$ , with RDF analysis showing excellent agreement with AIMD references for all atomic pair correlations (see Appendix A for detailed analysis). While all models maintain stable thermodynamic ensembles at 600K (Fig. 1c), the zero-shot foundation model exhibits a persistent pressure offset, likely due to its training on 0K equilibrium structures rather than finite-temperature configurations.

Despite similar performance on local structural (RDF) and short-time dynamic (VACF) properties, the models diverge significantly in their predictions of long-timescale transport phenomena. Fine-tuned models predict higher diffusion coefficients than both foundation and scratch models (Fig. 1e), with the multi-temperature fine-tuned variant showing the largest enhancement. This suggests that exposure to high-temperature

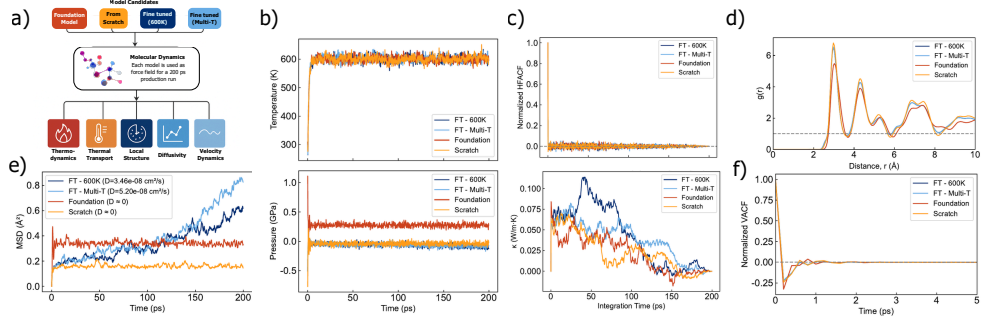


**Fig. 1: Comprehensive Benchmarking of MLFF Performance in Molecular Dynamics Simulations.** (a) A schematic of the unified evaluation protocol. Four candidate models—a zero-shot foundation model, a bespoke model trained from scratch, and two fine-tuned variants—are each used to drive a 200 ps molecular dynamics simulation. The resulting trajectories are then subjected to a uniform set of post-processing analyses to evaluate key physical properties. (b) Thermal transport properties, showing the Heat Flux Autocorrelation Function (HFACF) and its running integral to compute thermal conductivity ( $\kappa$ ). (c) Thermodynamic stability, demonstrated by the evolution of temperature and pressure over the simulation, which remain stable around their target values for all models. (d) The Total Radial Distribution Function (RDF),  $g(r)$ , revealing the local atomic structure. (e) The Mean Squared Displacement (MSD), used to assess atomic mobility and calculate the diffusion coefficient. (f) The Velocity Autocorrelation Function (VACF), which describes the system’s underlying dynamics.

training data creates a flatter potential energy (PES) that persists even at lower temperatures.

Notably, thermal conductivity calculations reveal differences in how models capture collective vibrational modes. The foundation model’s thermal conductivity decays rapidly toward zero, failing to sustain the long-range phonon correlations characteristic of the crystalline structure. In contrast, models trained or fine-tuned on system-specific data maintain these correlations, though the 600K-only model exhibits an anomalous peak suggesting potential structural instability. These results demonstrate that validating MLFFs solely on static structures and short-time dynamics is insufficient—a comprehensive assessment must include transport properties that probe long-range, collective phenomena.

### 3.2 Benchmarking the MLFF for Non-Equilibrium Diffusion Pathways

A rigorous test of the generalizability of a machine learning force field extends beyond its ability to reproduce thermodynamic properties. It must also accurately describe the potential energy surface (PES) in regions far from the training data’s energetic minima, such as the high-energy transition states that govern kinetic processes. To this end, we evaluated the performance of our MACE model on the challenging task of predicting the diffusion barrier for a fundamental migration event in the Cr-doped

$\text{Sb}_2\text{Te}_3$  system. This task is substantially more demanding than constant-temperature MD simulations (e.g., at 600 K), as it requires the model to capture not only accurate energies, but also the subtle curvature of the PES at a first-order saddle point—a stringent test of the model’s learned representation of interatomic interactions.

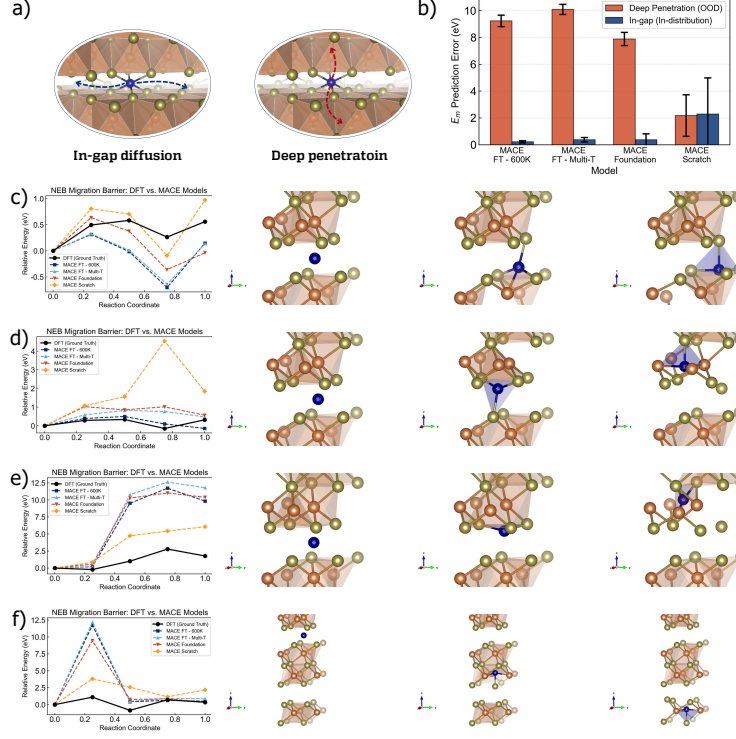


**Fig. 2: Comparative analysis of MLFF training strategies for predicting atomic migration barriers.** (a) Schematic illustration of the simulated Cr atom migration pathway between two stable sites within the  $\text{Sb}_2\text{Te}_3$  bilayer. (b) Bar plot showing the migration energy prediction errors for various models, spanning bespoke training to advanced active learning approaches. (c–f) Comparison of the minimum energy pathway (MEP) profiles for the Cr migration process. The solid black line denotes the ground-truth DFT reference, while dashed lines represent predictions from MACE models trained with different strategies.

### 3.3 Quantitative Comparison of Migration Barriers

To perform a direct and controlled evaluation of the learned PES for each model, we used the minimum energy pathway (MEP) obtained from our reference DFT nudged elastic band (NEB) calculation as a fixed geometric trajectory. By calculating the single-point energy for each of these pre-defined images, we can decouple the model’s

energetic accuracy from its structural relaxation behavior, providing a direct probe of its ability to describe the reaction pathway.

Our DFT calculations, serving as the ground-truth reference, establish a migration energy barrier ( $E_a$ ) of 0.34 eV for this process. The results, presented in Fig. 2d, reveal a clear hierarchy in performance and highlight the considerable impact of training strategy on the prediction of kinetic barriers. The two baseline strategies—training from scratch and using the zero-shot foundation model—demonstrate the fundamental challenges of specialization and generalization. The MACE Scratch model, despite being trained on a comprehensive in-house dataset, exhibits a catastrophic failure in predicting the barrier, overestimating the activation energy by over 4 eV. This is a classic signature of poor extrapolation. Even with tens of thousands of AIMD frames, the high-energy, low-probability configurations corresponding to the transition state are insufficiently sampled. Consequently, the model overfits to the more prevalent, near-equilibrium states and fails dramatically when asked to evaluate this critical, out-of-distribution rare event.

Conversely, the MACE Foundation model provides a qualitatively plausible prediction, capturing the smooth, convex shape of the energy barrier. This is a testament to the power of pre-training on millions of diverse structures; the model has learned a general understanding of physical interactions. However, it is quantitatively inaccurate, overestimating the barrier by approximately 0.7 eV—an unacceptably high amount—and misplacing the transition state along the reaction coordinate. This behavior is characteristic of a “softened” or “averaged” potential energy surface, a known trait of foundation models trained to generalize across vast chemical spaces. While broadly correct, the foundation model lacks the sharp, system-specific features of the true PES for Cr:Sb<sub>2</sub>Te<sub>3</sub>, effectively smoothing over the precise details required for high-fidelity kinetic predictions. The pronounced failures of these two baseline strategies underscore the necessity of a hybrid approach, motivating our investigation into fine-tuning.

### 3.3.1 The Critical Role of Task-Specific Fine-Tuning

The dramatic improvement seen in the fine-tuned models underscores the necessity of specializing the foundation model’s knowledge. The MACE FT-600K model, fine-tuned specifically on data generated at the target temperature of the migration event, achieves remarkable accuracy, with a barrier error of only 0.16 eV. This demonstrates that targeted fine-tuning effectively “sharpens” the softened PES of the foundation model. By providing a small but highly relevant set of in-domain data, we enable the model to learn the specific local atomic interactions required to accurately resolve the transition state structure and energy.

Intriguingly, the MACE FT-Multi-T model, which was fine-tuned on a larger and more diverse dataset spanning multiple temperatures, yields a less accurate barrier than the model trained at a specific temperature, here 600 K. While its predictions for the initial and final states (the thermodynamic endpoints) are accurate, its description of the kinetic barrier is a compromise, retaining some of the “softened” character of the original foundation model. This leads to an important insight: for MLFFs, more data is not axiomatically better. The relevance of the fine-tuning data

to the specific task is paramount. For predicting thermodynamic properties, a multi-temperature dataset is superior. For predicting a specific kinetic process, a dataset rich in configurations relevant to that process’s temperature regime is more effective. These findings collectively highlight a critical challenge in the practical application of MLFFs. The failure of the from-scratch model illustrates the difficulty of adequately sampling rare events, while the inaccuracies of the foundation model reveal the limitations of a purely generalist approach.

The success of targeted fine-tuning points the way forward, but the divergent results of the 600K and Multi-T models prove that the data selection process is non-trivial. This motivates the need for more advanced methods, such as the uncertainty-guided active learning explored in our work, which can intelligently identify and acquire the most informative data to improve model robustness and accuracy in a data-efficient manner.

### 3.3.2 Further Testing Different Trajectories

To probe the generalization capabilities of the different MLFF training strategies, we evaluated their performance on two distinct Cr migration pathways (Fig. ??a) with fundamentally different characteristics. The first pathway, *in-gap diffusion*, involves Cr migration within the van der Waals (vdW) gap between  $\text{Sb}_2\text{Te}_3$  quintuple layers, with low energy barriers and configurations similar to the training data, thereby testing interpolative accuracy.

In contrast, the second pathway, *deep penetration*, requires the Cr atom to move vertically from the vdW gap and penetrate directly into the interior of a QL, ultimately reaching a deeply buried site within the layer. This migration path is associated with significantly higher energy barriers and accesses high-distortion configurations that are not well-represented in the training data—making it an out-of-distribution (OOD) scenario with potentially more metastable configurations along the pathway. Testing both pathways allows us to evaluate model accuracy on familiar configurations and extrapolative power in challenging regions of the configuration space.

### 3.3.3 In-Gap Diffusion: A Test of Interpolative Accuracy

For the in-gap diffusion pathway (Fig. 2c–d), where the Cr atom moves within the van der Waals gap or just shallowly penetrates the interface, the atomic environments along the minimum energy path (MEP) are reasonably similar to the near-equilibrium states sampled during the AIMD simulations. In this regime, the performance hierarchy is clear. The fine-tuned models, particularly MACE FT-600K, demonstrate excellent agreement with the DFT reference, accurately predicting both the thermodynamic endpoints and the kinetic barrier (Fig. 2d). This success highlights that, when the task lies within the domain of the training data, fine-tuning effectively “sharpens” the generalist foundation model’s potential energy surface (PES) to capture system-specific details. In contrast, the MACE Scratch model, despite being trained on the same data, fails significantly, underscoring its inability to learn the subtle energy differences required to resolve the transition state from a limited dataset.



### 3.3.4 Deep Penetration: A Test of Extrapolative Robustness

The “deep penetration” pathway provides a much more stringent test of model robustness. This path involves significant lattice distortion as the Cr atom pushes its way through the covalently bonded quintuple layer (QL), creating atomic environments that are far from those seen in the training data (Fig. 2a).

While the fine-tuned and foundation models remain accurate for the stable initial and final states (an interpolative task), they fail catastrophically in predicting the energy of the transition state, overestimating the barrier by a large margin. This is a classic example of out-of-distribution failure, where the inductive biases learned from near-equilibrium data do not generalize to highly distorted, high-energy configurations. The models have learned to be a “materials expert” for stable structures but remain a “naïve physicist” for unseen, strained states.

The MACE Scratch model, which performed least well of the four models on the in-gap pathway, yields the lowest barrier error for this out-of-distribution task (Fig. 2e, f). This is not because the scratch model is “better”; rather, its globally inaccurate and likely unphysical PES happens, by chance, to be less pathologically incorrect in this specific high-energy region than the foundation model’s PES. The pre-trained model’s failure suggests that its supposedly general knowledge contains strong implicit assumptions about near-equilibrium physics that break down dramatically when extrapolating.

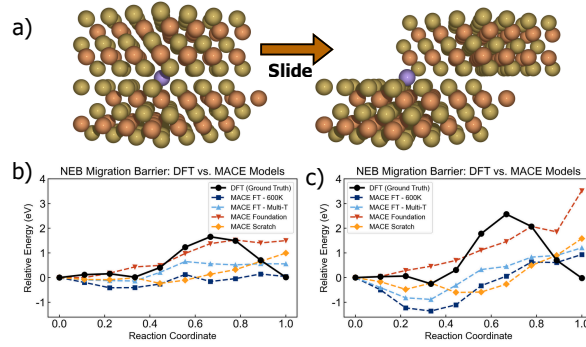


**Fig. 3: Evaluation of MACE models on collective lattice displacement: interlayer sliding in  $\text{Sb}_2\text{Te}_3$ .** (a) Schematic illustration of the bilayer sliding process in  $\text{Sb}_2\text{Te}_3$ , where the top layer (yellow/orange atoms) slides relative to the bottom layer along the crystallographic direction. The purple sphere indicates the position of a Cr dopant when present. (b) Energy barriers for interlayer sliding in pristine  $\text{Sb}_2\text{Te}_3$  as calculated by DFT (black, ground truth) and various MACE models. The reaction coordinate represents the normalized sliding distance from the initial to final configuration. (c) Energy barriers for the same sliding process in Cr-doped  $\text{Sb}_2\text{Te}_3$ .



### 3.4 Interlayer Sliding: Probing Robustness to Non-Local, Collective Displacements

Having tested the models’ response to local, high-distortion events, we evaluated their robustness to a different class of out-of-distribution challenge: large-scale, collective lattice displacements. To this end, we simulated the shearing of one  $\text{Sb}_2\text{Te}_3$  layer relative to the other, a process governed by the subtle corrugations of the interlayer van der Waals potential energy surface (Fig. 3a). This task is particularly challenging for MLFFs as the local atomic environment of any given atom changes only minimally, while the global configuration undergoes a significant transformation that crosses periodic boundaries. The configurations along this sliding path were not present in the training data.

We first examined the case of pure, undoped  $\text{Sb}_2\text{Te}_3$  (Fig. 3b). The results reveal a clear trade-off between the models. The MACE Foundation model provides the most reasonable estimate of the energy barrier’s shape and magnitude, suggesting its vast pre-training on bulk crystals has endowed it with a better implicit understanding of such periodic, mechanical deformations. However, it fails to maintain translational symmetry, incorrectly predicting the final state to be higher in energy than the identical initial state. This energy drift is a clear artifact, indicating a failure to perfectly respect the periodic nature of the simulation cell under large displacements. The MACE Scratch model exhibits a similar version of this artifact.

Conversely, the fine-tuned models (MACE FT-600K and Multi-T) significantly underestimate the energy barrier. This suggests a compelling hypothesis: the process of fine-tuning, while “sharpening” the PES for local chemistry around the Cr dopant, has degraded the model’s learned representation of the weaker, long-range interlayer physics inherited from the foundation model. The optimization has prioritized local accuracy at the expense of non-local, collective interactions.

This trend is largely mirrored in the Cr-doped system (Fig. 3c), confirming that this is a fundamental behavior of the models rather than an effect specific to the dopant. The failure of all models to perfectly capture both the barrier height and the endpoint periodicity highlights a key limitation of local-descriptor-based MLFFs. Phenomena like shearing, stacking faults, and dislocation glide are inherently non-local. While the models excel at describing local bonding and coordination, they can struggle to enforce long-range physical constraints that extend beyond their cutoff radius. This underscores the need for careful validation when using standard MLFFs to study mechanical properties and points towards future work in developing training sets that explicitly include these collective deformation modes or exploring architectures designed to capture long-range physics more effectively.

### 3.5 Representation Learning Analysis

To elucidate the origins of the observed performance differences, we conducted an analysis of the learned representations by projecting the high-dimensional atomic environment descriptors from each model into a two-dimensional space using t-distributed stochastic neighbor embedding (t-SNE), as shown in Fig. 4. This visualization reveals

striking differences in how models trained with different strategies encode the same physical system.

The MACE Foundation and MACE Scratch models occupy distinct, well-separated regions of the latent space, as illustrated in the cross-model overlay (Fig. 4c) and quantified by high average silhouette scores (Fig. 4d). The foundation model’s representations are relatively compact, reflecting a generalist encoding trained to be robust across a vast chemical space. In contrast, the scratch-trained model produces a more dispersed representation, suggesting it has learned highly specific features to differentiate configurations within our limited in-house dataset; this specialization may contribute to its poor generalization on out-of-distribution tasks, such as NEB pathways.

Crucially, the representations of the two fine-tuned models (FT-600K and FT-Multi-T) are not only similar to each other (Fig. 4a, b) but also occupy a region of the latent space intermediate between the foundation and scratch models (Fig. 4c). This provides a powerful insight into the mechanism of fine-tuning: it effectively pulls the generalist representations of the foundation model towards the specialized representations required for the new task. Since fine-tuning begins with the foundation model’s weights and proceeds with the same in-house data used to train the scratch model, the resulting learned representations manifest as a hybrid.

This “hybrid representation” explains the balanced performance of the fine-tuned models. They retain sufficient general knowledge from the foundation model to remain stable and perform well on non-local tasks, while also incorporating specialized features from the in-house dataset that enable accurate prediction of system-specific properties, such as the in-gap migration barrier—outperforming both of the baseline models on that task. This finding underscores that model performance differences arise not from minor parameter adjustments, but from qualitatively distinct learned representations of the underlying material physics.

## 4 Conclusion

We benchmarked specialist (from-scratch) and generalist (foundation-based) machine-learned force fields (MLFFs) for Cr-intercalated  $\text{Sb}_2\text{Te}_3$ , emphasizing migration pathways as a diagnostic probe. NEB trajectories revealed that, while all models reproduce equilibrium structures, their performance diverges sharply for kinetic tasks. Migration thus provides a generalizable benchmark that tests both interpolation and extrapolation, exposing weaknesses invisible to equilibrium-only validation.

Our results address the core questions posed in the introduction. First, both from-scratch and zero-shot foundation models fail for migration barriers: the former struggles with extrapolation, while the latter produces overly averaged potentials. Second, task-specific fine-tuning recovers kinetic accuracy, but at the cost of degraded performance for long-range physics such as interlayer sliding. Third, latent-space analysis shows these paradigms encode fundamentally distinct, non-overlapping physical representations, explaining hidden extrapolation failures.

These findings reframe the specialist vs. generalist debate: the choice is not just about efficiency but about qualitatively different physics learned by each model. Migration-based probes, coupled with latent-space diagnostics, offer a practical route

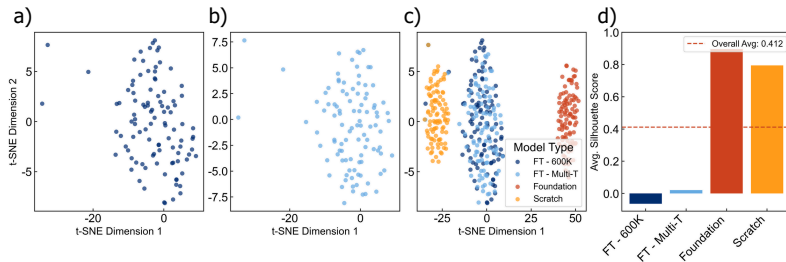


**Fig. 4: Representation learning analysis reveals distinct atomic environment encodings across training strategies.** Two-dimensional t-SNE projections of atomic environment descriptors extracted from 600 K molecular dynamics trajectories. (a) The latent space embedding for the FT-600K model. (b) The embedding for the FT-Multi-T model, showing a similar distribution to the FT-600K model. (c) A cross-model overlay of representations from all four strategies. The foundation (red) and scratch-trained (orange) models occupy distinct, well-separated regions of the latent space. The fine-tuned models (dark and light blue) occupy an intermediate region, demonstrating that fine-tuning adapts the generalist representations towards the specialist domain. (d) Average silhouette scores for each model’s cluster relative to the others.

to uncover hidden failures and guide uncertainty-aware active learning. This framework has the potential to generalize beyond the present case, enabling more robust and data-efficient MLFF development for accelerated materials discovery.

## References

- [1] Zhang, H., Liu, C.-X., Qi, X.-L., Dai, X., Fang, Z., Zhang, S.-C.: Topological insulators in Bi<sub>2</sub>Se<sub>3</sub>, Bi<sub>2</sub>Te<sub>3</sub> and Sb<sub>2</sub>Te<sub>3</sub> with a single Dirac cone on the surface. *Nature Physics* **5**(6), 438–442 (2009) <https://doi.org/10.1038/nphys1270> . Publisher: Nature Publishing Group. Accessed 2025-02-12
- [2] Guo, Y., Liu, Z., Peng, H.: A Roadmap for Controlled Production of Topological Insulator Nanostructures and Thin Films. *Small* **11**(27), 3290–3305 (2015) <https://doi.org/10.1002/sml.201403426> . eprint: <https://onlinelibrary.wiley.com/doi/pdf/10.1002/sml.201403426>. Accessed 2025-05-15
- [3] Cortie, D., Zhao, W., Yue, Z., Li, Z., Bake, A., Marenych, O., Pastuovic, Z., Nancarrow, M., Zhang, Z., Qi, D.-C., Evans, P., Mitchell, D.R.G., Wang, X.: Creating thin magnetic layers at the surface of Sb<sub>2</sub>Te<sub>3</sub> topological insulators using a low-energy chromium ion beam. *Applied Physics Letters* **116**(19), 192410 (2020) <https://doi.org/10.1063/5.0006447> . Accessed 2024-11-13
- [4] Han, M.-K., Ryu, H., Kim, S.-J.: Effect of Chromium Doping on the Thermoelectric Properties of Bi<sub>2</sub>Te<sub>3</sub>: Cr<sub>x</sub>Bi<sub>2</sub>Te<sub>3</sub> and Cr<sub>x</sub>Bi<sub>2-x</sub>Te<sub>3</sub>. *Journal of Electronic Materials*

- 42**(9), 2758–2763 (2013) <https://doi.org/10.1007/s11664-013-2670-4> . Accessed 2025-03-16
- [5] A. Deus, D.P., Oliveira, I.S.S., Oliveira, J.B., Scopel, W.L., Miwa, R.H.: Magnetic switch and electronic properties in chromium-intercalated two-dimensional  $\text{GeP}_3$ . *Physical Review Materials* **5**(5), 054002 (2021) <https://doi.org/10.1103/PhysRevMaterials.5.054002> . Publisher: American Physical Society. Accessed 2025-07-24
  - [6] Kohn, W., Sham, L.J.: Self-Consistent Equations Including Exchange and Correlation Effects. *Physical Review* **140**(4A), 1133–1138 (1965) <https://doi.org/10.1103/PhysRev.140.A1133> . Publisher: American Physical Society. Accessed 2025-08-20
  - [7] Perdew, J.P., Burke, K., Ernzerhof, M.: Generalized Gradient Approximation Made Simple. *Physical Review Letters* **77**(18), 3865–3868 (1996) <https://doi.org/10.1103/PhysRevLett.77.3865> . Publisher: American Physical Society. Accessed 2024-11-01
  - [8] Sohler, T., Calandra, M., Mauri, F.: Density functional perturbation theory for gated two-dimensional heterostructures: Theoretical developments and application to flexural phonons in graphene. *Physical Review B* **96**(7), 075448 (2017) <https://doi.org/10.1103/PhysRevB.96.075448> . Publisher: American Physical Society. Accessed 2025-03-19
  - [9] Choudhary, K., Kalish, I., Beams, R., Tavazza, F.: High-throughput Identification and Characterization of Two-dimensional Materials using Density functional theory. *Scientific Reports* **7**(1), 5179 (2017) <https://doi.org/10.1038/s41598-017-05402-0> . Publisher: Nature Publishing Group. Accessed 2024-11-19
  - [10] Unke, O.T., Chmiela, S., Sauceda, H.E., Gastegger, M., Poltavsky, I., Schütt, K.T., Tkatchenko, A., Müller, K.-R.: Machine Learning Force Fields. *Chemical Reviews* **121**(16), 10142–10186 (2021) <https://doi.org/10.1021/acs.chemrev.0c01111> . Publisher: American Chemical Society. Accessed 2025-05-15
  - [11] Batatia, I., Kovács, D.P., Simm, G.N.C., Ortner, C., Csányi, G.: MACE: Higher Order Equivariant Message Passing Neural Networks for Fast and Accurate Force Fields
  - [12] Batzner, S., Musaelian, A., Sun, L., Geiger, M., Mailoa, J.P., Kornbluth, M., Molinari, N., Smidt, T.E., Kozinsky, B.: E(3)-equivariant graph neural networks for data-efficient and accurate interatomic potentials. *Nature Communications* **13**(1), 2453 (2022) <https://doi.org/10.1038/s41467-022-29939-5> . Publisher: Nature Publishing Group. Accessed 2024-12-22
  - [13] Zeng, J., Zhang, D., Lu, D., Mo, P., Li, Z., Chen, Y., Rynik, M., Huang, L., Li, Z., Shi, S., Wang, Y., Ye, H., Tuo, P., Yang, J., Ding, Y., Li, Y., Tisi, D., Zeng, Q., Bao, H., Xia, Y., Huang, J., Muraoka, K., Wang, Y., Chang, J., Yuan, F., Bore,

- S.L., Cai, C., Lin, Y., Wang, B., Xu, J., Zhu, J.-X., Luo, C., Zhang, Y., Goodall, R.E.A., Liang, W., Singh, A.K., Yao, S., Zhang, J., Wentzcovitch, R., Han, J., Liu, J., Jia, W., York, D.M., E, W., Car, R., Zhang, L., Wang, H.: DeePMD-kit v2: A software package for deep potential models. *The Journal of Chemical Physics* **159**(5), 054801 (2023) <https://doi.org/10.1063/5.0155600> . Accessed 2024-12-15
- [14] Wines, D., Choudhary, K.: CHIPS-FF: Evaluating Universal Machine Learning Force Fields for Material Properties. *ACS Materials Letters*, 2105–2114 (2025) <https://doi.org/10.1021/acsmaterialslett.5c00093> . Publisher: American Chemical Society. Accessed 2025-05-11
- [15] Deng, B., Zhong, P., Jun, K., Riebesell, J., Han, K., Bartel, C.J., Ceder, G.: CHGNet as a pretrained universal neural network potential for charge-informed atomistic modelling. *Nature Machine Intelligence* **5**(9), 1031–1041 (2023) <https://doi.org/10.1038/s42256-023-00716-3> . Publisher: Nature Publishing Group. Accessed 2025-08-01
- [16] Yang, H., Hu, C., Zhou, Y., Liu, X., Shi, Y., Li, J., Li, G., Chen, Z., Chen, S., Zeni, C., Horton, M., Pinsler, R., Fowler, A., Zügner, D., Xie, T., Smith, J., Sun, L., Wang, Q., Kong, L., Liu, C., Hao, H., Lu, Z.: MatterSim: A Deep Learning Atomistic Model Across Elements, Temperatures and Pressures. *arXiv*. arXiv:2405.04967 [cond-mat] (2024). <https://doi.org/10.48550/arXiv.2405.04967> . <http://arxiv.org/abs/2405.04967> Accessed 2025-04-30
- [17] Wood, B.M., Dzamba, M., Fu, X., Gao, M., Shuaibi, M., Barroso-Luque, L., Abdelmaqsoud, K., Gharakhanyan, V., Kitchin, J.R., Levine, D.S., Michel, K., Sriram, A., Cohen, T., Das, A., Rizvi, A., Sahoo, S.J., Ulissi, Z.W., Zitnick, C.L.: UMA: A Family of Universal Models for Atoms. *arXiv*. arXiv:2506.23971 [cs] (2025). <https://doi.org/10.48550/arXiv.2506.23971> . <http://arxiv.org/abs/2506.23971> Accessed 2025-08-20
- [18] Dunn, A., Wang, Q., Ganose, A., Dopp, D., Jain, A.: Benchmarking materials property prediction methods: the Matbench test set and Automatminer reference algorithm. *npj Computational Materials* **6**(1), 138 (2020) <https://doi.org/10.1038/s41524-020-00406-3> . Publisher: Nature Publishing Group. Accessed 2025-08-12

## A Detailed Computational Methods

### A.1 First-Principles Reference Calculations

All reference data were generated using Density Functional Theory (DFT) as implemented in the Quantum Espresso simulation package. We employed ultrasoft pseudopotentials for all elements (Cr, Sb, Te) with a plane-wave kinetic energy cut-off of 400 eV. The Brillouin zone was sampled using a Monkhorst-Pack k-point grid of  $4 \times 4 \times 1$  for structural relaxations and Nudged Elastic Band (NEB) calculations. The Perdew-Burke-Ernzerhof (PBE) exchange-correlation functional was used, which we have found in prior investigations to provide a reliable balance of computational efficiency and accuracy for this class of materials.

The training dataset was generated from ab initio molecular dynamics (AIMD) simulations performed in the NVT ensemble using a Langevin thermostat. These simulations covered a range of temperatures (300 K, 600 K, 1200 K) and Cr doping concentrations to ensure the model was exposed to a diverse set of thermodynamic and structural configurations. Each AIMD trajectory was run for 10 ps on a system of 120 atoms. To investigate the nature of atomic migration pathways, minimum energy paths (MEPs) and energy barriers were calculated using the Nudged Elastic Band (NEB) method. All initial, final, and intermediate configurations were considered to be converged when the forces on all unconstrained atoms fell below 0.01 eV/Å.

### A.2 MACE Model Training Protocols

#### A.2.1 Training Hyperparameters

All training and fine-tuning procedures were executed with a consistent set of hyperparameters to ensure fair comparison:

- Optimizer: Adam
- Initial learning rate:  $1 \times 10^{-3}$
- Batch size: 4
- Early stopping: Implemented based on validation set Force MAE
- Maximum epochs: 1000
- Validation split: 10% of training data

#### A.2.2 Fine-Tuning Details

For the FT-600K model, we selected a representative 5% subset (approximately 1,000 configurations) from the 600K AIMD trajectories. The subset was chosen to capture the full range of structural variations observed at this temperature, including both equilibrium fluctuations and transitional configurations.

For the FT-Multi-T model, the training subset was composed equally from 300K, 600K, and 1200K trajectories, ensuring exposure to diverse thermal conditions. The multi-temperature dataset was designed to test whether broader thermodynamic sampling improves generalization.

The choice of 600K for single-temperature fine-tuning represents typical thermoelectric operating temperatures, reflecting realistic usage conditions. At roughly two-thirds

of  $\text{Sb}_2\text{Te}_3$ ’s melting point, this temperature captures significant thermal dynamics without structural deterioration.

Fine-tuning foundation models for specific chemical systems presents a fundamental challenge: how to adapt to new domains while preserving learned representations. This document discusses our fine-tuning strategy.

### A.2.3 Fine-tuning Underlying Mechanism

In fine-tuning, the pre-trained model parameters  $\theta_0$  are directly optimized on the target dataset  $\mathcal{D}_{\text{target}}$ :

$$\theta^* = \arg \min_{\theta} \mathcal{L}(\theta; \mathcal{D}_{\text{target}}) \quad (1)$$

#### *Characteristics*

- **Simple implementation:** Direct optimization on new data
- **Fast convergence:** High learning rate ( $\alpha \sim 10^{-2}$ )
- **Catastrophic forgetting:** Loss of original capabilities
- **Single objective:** Optimizes only for target domain performance

### A.2.4 Implementation Details

#### A.2.5 Practical Considerations

##### *When to Use Fine-tuning*

- Limited computational resources
- Domain-specific applications only
- Rapid prototyping requirements
- No need for generalization beyond the target dataset

##### *Take-away*

Fine-tuning offers rapid adaptation to new datasets with relatively low computational cost. However, this comes at the expense of catastrophic forgetting, where the model loses its original generalization capabilities.

## B Supplementary Materials

### B.1 MACE Model Performance Evaluation by RMSE

All developed Machine-Learned Force Fields (MLFFs) demonstrate high fidelity in predicting energies and forces, as illustrated by the parity plots in Figure 5, which compare model predictions to the reference DFT calculations. The performance of each model across the training, validation, and test sets is quantitatively summarized in Table 1. As detailed in the table, the models fine-tuned from the foundation model show a marked improvement over the model trained from scratch, with energy and force Root Mean Square Errors (RMSEs) being significantly reduced on the independent test set.



**Table 1:** Performance metrics for MACE models across training, validation, and test sets. The FT-600K metrics are the mean  $\pm$  standard deviation across three independent training runs with different random seeds.

Model	Train RMSE F (meV/Å)	Valid RMSE F (meV/Å)	Test RMSE F (meV/Å)	Test RMSE E (meV/atom)
From Scratch	67.1	76.1	75.2	1.0
FT-600K	$20.7 \pm 11.8$	$44.6 \pm 2.9$	$37.2 \pm 0.6$	$0.5 \pm 0.0$
FT-MultiT	20.3	49.1	45.5	0.5

A deeper analysis of the training dynamics reveals important characteristics of the models. The model trained from scratch exhibits a relatively small gap between training (67.1 meV/Å) and validation (76.1 meV/Å) force RMSEs. While this suggests only moderate overfitting, its high error across all datasets indicates that it underfits the true physical interactions.

In contrast, the fine-tuned models display a more pronounced overfitting behavior, characterized by a large gap between their low training RMSEs and higher validation RMSEs. For instance, the FT-MultiT model shows a 142% increase in force RMSE from the training (20.3 meV/Å) to the validation set (49.1 meV/Å). This aggressive fitting is expected when fine-tuning on smaller, more specialized datasets. The high standard deviation in the FT-600K model’s training RMSE (11.8 meV/Å) also suggests a sensitivity to initialization during the training process.

Despite the strong overfitting signals, the fine-tuned models generalize well to the test set, outperforming the scratch model by a significant margin. This analysis reinforces the central argument of our work: standard accuracy metrics like RMSE are insufficient for a comprehensive evaluation of MLFFs. While these metrics and the parity plots in Figure 5 confirm the models’ general accuracy, they do not capture critical performance on physical properties such as energy barriers and transport phenomena, necessitating the more extensive, property-driven benchmarks presented in the main text.

## B.2 Detailed Structural and Thermodynamic Analysis

The RDF analysis reveals that all MACE models, regardless of training strategy, successfully reproduce the key structural features of the Cr-doped Sb<sub>2</sub>Te<sub>3</sub> system when compared to the AIMD ground truth (Fig. 6b).

All models correctly capture the primary coordination shells, with the first peak positions for Cr–Cr, Cr–Sb, and Cr–Te pairs occurring at approximately 3.0 Å, 3.2 Å, and 2.8 Å, respectively, in excellent agreement with the AIMD reference. The peak heights and positions remain consistent across all training strategies (Figures 6c–f), indicating that the local atomic structure is well preserved regardless of whether the model was trained from scratch, used as a foundation model, or fine-tuned with temperature-specific data.

The primary observable difference between models lies in the smoothness of the RDF curves rather than their fundamental features. The scratch-trained model (Fig. 6d)

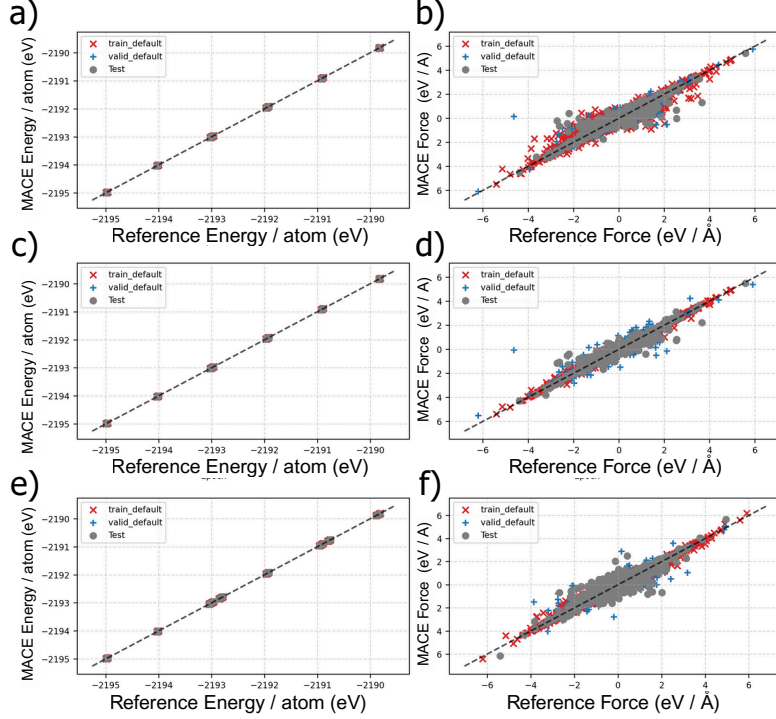


**Fig. 5: Parity plots comparing MACE-predicted energies and forces against DFT reference calculations for the test set.** (a, b) Model trained from scratch, (c, d) fine-tuned 600 K model (“FT-600K”), and (e, f) fine-tuned multi-temperature model (“FT-MultiT”). Parity plots for energies (a, c, e) demonstrate excellent agreement for all models, while force parity plots (b, d, f) show strong overall correlation but subtle differences in error distributions that are not distinguishable visually. These results highlight the necessity of quantitative and property-based benchmarks for robust model evaluation.

exhibits slightly smoother RDF profiles compared to the fine-tuned variants (Figures 6e–f). This difference arises from practical computational considerations rather than fundamental accuracy: the scratch model, being more compact with fewer parameters, allowed for longer MD trajectories within the same computational budget, resulting in better statistical sampling. In contrast, the fine-tuned models, while maintaining larger parameter counts from their foundation architectures, required more computational resources per MD step, limiting the total simulation time and resulting in slightly noisier RDF profiles.

Notably, both fine-tuning strategies—whether using single-temperature (600 K) or multi-temperature AIMD data—produce nearly identical RDF profiles, suggesting that the structural representation of the material is robust to the temperature range of the training data. This indicates that, for structural properties, the choice of training

strategy has minimal impact, with all approaches converging to similar descriptions of the local atomic environment. The preservation of accurate structural features across all models provides confidence that the learned interatomic potentials correctly capture the fundamental bonding characteristics of the Cr-doped  $\text{Sb}_2\text{Te}_3$  system.

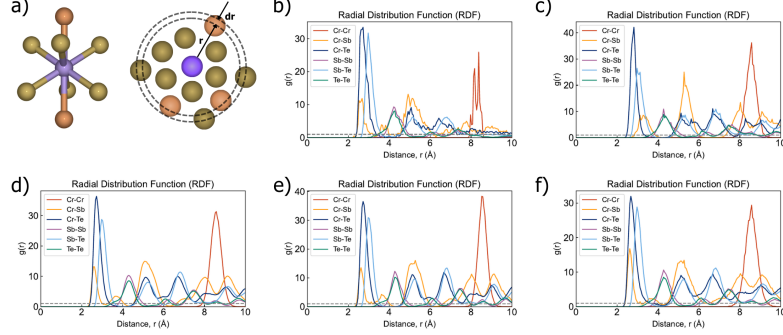


**Fig. 6: Radial distribution function (RDF) analysis of Cr-doped  $\text{Sb}_2\text{Te}_3$  at 600 K.** (a) Schematic illustration of the local atomic environment around a Cr dopant (purple) in the  $\text{Sb}_2\text{Te}_3$  lattice, showing the first coordination shell of Te atoms (gold) and second-shell Sb atoms (orange). The dashed circles indicate the radial distances used for RDF calculation. (b-f) Computed RDFs for different atom pairs from molecular dynamics simulations: (b) Ab initio molecular dynamics (AIMD) ground truth reference, (c) MACE foundation model without fine-tuning, (d) MACE model trained from scratch on Cr- $\text{Sb}_2\text{Te}_3$  data, (e) MACE model fine-tuned with 600 K AIMD data (“FT - 600K”), and (f) MACE model fine-tuned with multi-temperature AIMD data (“FT - Multi-T”). All simulations were performed at 600 K with  $5 \times 5 \times 1$  supercells for 200 ps. The RDF peaks correspond to characteristic interatomic distances in the doped structure, with the first peak representing nearest-neighbor correlations.

### B.3 Thermodynamic Ensemble Stability

A detailed analysis of the pressure profiles reveals subtle but important differences between models. The zero-shot MACE Foundation model equilibrates to a slightly different average pressure than the models trained or fine-tuned on our in-house AIMD data. This is likely a consequence of the foundation model being trained on a vast dataset of materials at their 0K equilibrium volumes. A minor mismatch between the foundation model’s predicted equilibrium lattice parameters and the true DFT values for our specific Cr: $\text{Sb}_2\text{Te}_3$  system at 600K manifests as a persistent non-zero average pressure in an NVT simulation. The fine-tuned and scratch models, having been trained explicitly on data from this system’s true ensemble, do not exhibit this deviation.

## B.4 Transport Property Analysis

The divergence in transport properties provides deeper insights into model behavior. The enhanced diffusivity in multi-temperature fine-tuned models likely stems from their exposure to high-temperature configurations approaching disordered or liquid-like states during training. By learning from these states, the model may have developed a potential energy surface that is slightly "flatter" or has lower barriers to diffusion, an effect that persists even at the 600K simulation temperature.

The thermal conductivity analysis reveals even more fundamental differences. The rapid decay of thermal conductivity in the foundation model indicates a failure to sustain long-range heat-carrying vibrational modes (phonons) specific to this crystalline structure. The anomalous peak observed in the 600K-only fine-tuned model's HFACF during the first 50 ps suggests potential structural instability or abrupt structural changes that alter phonon behavior. This highlights how different training strategies can lead to qualitatively different representations of collective phenomena, even when local properties appear identical.

## B.5 Molecular Dynamics Simulations

### B.5.1 Simulation Protocol

MD simulations were performed using the Atomic Simulation Environment (ASE) with the following protocol:

- **Integrator:** Langevin dynamics for NVT ensemble or Nosé-Hoover for NPT ensemble
- **Timestep:** 1.0 fs
- **Friction coefficient:**  $\gamma = 0.01 \text{ fs}^{-1}$  (Langevin)
- **Barostat parameters:**  $\tau_p = 1000 \text{ fs}$ ,  $P = 1 \text{ bar}$  (NPT only)
- **Equilibration:** 50,000 steps (50 ps)
- **Production:** 200,000 steps (200 ps) for property calculations
- **Sampling interval:** Every 100 steps for analysis
- **System size:**  $5 \times 5 \times 1$  supercell (2050 atoms)

Simulations were conducted at two temperatures: 300 K and 600 K, to assess model performance under different thermal conditions. Initial velocities were assigned according to the Maxwell-Boltzmann distribution with removal of center-of-mass motion and angular momentum.

## B.6 Property Calculations

### B.6.1 Structural Properties

The radial distribution function (RDF)  $g(r)$  was computed for all unique atom pairs:

$$g_{\alpha\beta}(r) = \frac{V}{4\pi r^2 \Delta r N_\alpha N_\beta} \left\langle \sum_{i \in \alpha} \sum_{j \in \beta} \delta(r - r_{ij}) \right\rangle \quad (2)$$

where  $\alpha$  and  $\beta$  denote atomic species,  $V$  is the system volume,  $N_\alpha$  is the number of atoms of species  $\alpha$ , and the angle brackets denote time averaging.

### B.6.2 Dynamic Properties

The mean square displacement (MSD) was calculated for each atomic species:

$$\text{MSD}_\alpha(t) = \left\langle \frac{1}{N_\alpha} \sum_{i \in \alpha} |\mathbf{r}_i(t) - \mathbf{r}_i(0)|^2 \right\rangle \quad (3)$$

Diffusion coefficients were extracted from the linear regime of MSD using the Einstein relation:

$$D_\alpha = \lim_{t \rightarrow \infty} \frac{\text{MSD}_\alpha(t)}{6t} \quad (4)$$

The velocity autocorrelation function (VACF) was computed as:

$$C_v(t) = \frac{\langle \mathbf{v}(t) \cdot \mathbf{v}(0) \rangle}{\langle \mathbf{v}(0) \cdot \mathbf{v}(0) \rangle} \quad (5)$$

### B.6.3 Thermodynamic Properties

Average potential energy per atom, temperature, and volume (for NPT simulations) were calculated over the production phase:

$$\langle E \rangle = \frac{1}{N_{\text{frames}}} \sum_{i=1}^{N_{\text{frames}}} \frac{E_{\text{pot}}^{(i)}}{N_{\text{atoms}}} \quad (6)$$

with corresponding standard deviations to assess thermal fluctuations.

### B.6.4 Transport Properties

For thermal conductivity calculations, the heat flux vector was computed:

$$\mathbf{J} = \frac{1}{V} \left[ \sum_i e_i \mathbf{v}_i + \frac{1}{2} \sum_{i \neq j} (\mathbf{F}_{ij} \cdot \mathbf{v}_j) \mathbf{r}_{ij} \right] \quad (7)$$

where  $e_i$  is the per-atom energy,  $\mathbf{v}_i$  is the velocity,  $\mathbf{F}_{ij}$  is the force between atoms  $i$  and  $j$ , and  $\mathbf{r}_{ij}$  is their separation vector. The heat flux autocorrelation function (HFACF) was then computed for subsequent Green-Kubo analysis.

## B.7 Representation Learning Feature Extraction

The following physically interpretable descriptors were extracted from MD trajectories:

1. **Energy landscape:** Total potential energy per atom
2. **Force fields:** 3N-dimensional force vectors for all atoms
3. **Structural order parameters:** Radial distribution histograms computed with 100 bins up to 5.0 Å cutoff
4. **SOAP descriptors:** Smooth Overlap of Atomic Positions with:
  - Cutoff radius: 5.0 Å
  - Number of radial basis functions: 8

- Maximum angular momentum: 4
  - Gaussian width: 0.3 Å
5. **Mechanical response:** Numerical force derivatives with respect to 0.01 Å atomic displacements

These features were concatenated into a single vector per configuration, normalized, and projected using t-SNE (perplexity=30, learning rate=200) for visualization.

## B.8 Evaluation Metrics Definitions

- **Force MAE:**  $\frac{1}{3N} \sum_{i=1}^N \sum_{\alpha=x,y,z} |F_{i,\alpha}^{\text{MLFF}} - F_{i,\alpha}^{\text{DFT}}|$
- **Energy MAE:**  $\frac{1}{N} |E^{\text{MLFF}} - E^{\text{DFT}}|$
- **RMSD Growth Rate:** Linear fit slope of  $\text{RMSD}(t) = \sqrt{\frac{1}{N} \sum_{i=1}^N |\mathbf{r}_i(t) - \mathbf{r}_i(0)|^2}$
- **Silhouette Score:** Average of  $\frac{b_i - a_i}{\max(a_i, b_i)}$  where  $a_i$  is mean intra-cluster distance and  $b_i$  is mean nearest-cluster distance

## B.9 Detailed Migration Pathway Analysis

### B.9.1 In-Gap Diffusion

This pathway tests interpolative accuracy, as the atomic environments remain similar to equilibrium configurations in the training data. The clear performance hierarchy—with fine-tuned models excelling and scratch failing—validates that fine-tuning successfully “sharpens” the foundation model’s PES for in-domain predictions.

### B.9.2 Deep Penetration

This pathway creates severe lattice distortions as Cr pushes through covalently bonded layers, accessing configurations far from the training distribution. The universal failure at transition states, despite accurate endpoint predictions, reveals how models trained on near-equilibrium data develop strong inductive biases that break down for strained configurations.

The scratch model’s accidentally lower error on this OOD task is particularly instructive. Its globally inaccurate PES happens to be less catastrophically wrong in this specific high-energy region—not through physical insight but random chance. This underscores that the foundation model’s “general” knowledge contains implicit assumptions about equilibrium physics that fail dramatically under extrapolation.

### B.9.3 Implications for MLFF Development

These findings highlight critical considerations for practical MLFF deployment:

- **Validation Insufficiency:** Testing only on stable configurations masks critical failures at transition states
- **Hidden Extrapolation:** Models can appear accurate at trajectory endpoints while failing at crucial transition states
- **Data Quality over Quantity:** Task-specific training data outweighs larger but less relevant datasets

- **Foundation Model Limitations:** Pre-trained models require careful adaptation for processes involving significant atomic rearrangement

The results motivate advanced strategies like uncertainty-guided active learning that can identify high-uncertainty regions and intelligently augment training sets for improved extrapolative performance.

## B.10 Nudged Elastic Band (NEB) Benchmark for Cr Migration

To directly assess the practical performance of each model on a physically critical task, we performed a Nudged Elastic Band (NEB) calculation for a Cr atom migration event, as shown in Figure 7. This calculation serves as an effective and challenging probe to distinguish the models’ stability and predictive accuracy when exploring unseen transition-state geometries. The results reveal a dramatic difference in performance that is not apparent from the RMSE metrics alone.

Both the model trained from scratch and the fine-tuned models (FT-600K and FT-MultiT) exhibit explosive behavior during the NEB optimization, as evidenced by the sudden spike in the maximum force ( $f_{max}$ ) shown in Figure 7c. This instability forced the early termination of the calculations. This failure suggests that the interpolated images along the NEB path introduced metastable configurations, such as an unphysical separation of the material layers, which were outside the manifold of the training data. For the fine-tuned models, this indicates a form of catastrophic forgetting, where the models lost their generalized stability after being trained on a narrow dataset.

In contrast, the MACE foundation model, without any system-specific fine-tuning, successfully converged the NEB calculation. It predicts a migration barrier of 0.41 eV (Figure 7b), a value in good agreement with DFT calculations for similar in-gap diffusion pathways (0.3 eV). This level of accuracy, close to the bounds of chemical accuracy, demonstrates the foundation model’s exceptional capability to generalize to complex transition-state configurations. This benchmark underscores that evaluating performance on dynamic, physically relevant processes is a critical and necessary step for validating the true capabilities of MLFFs.



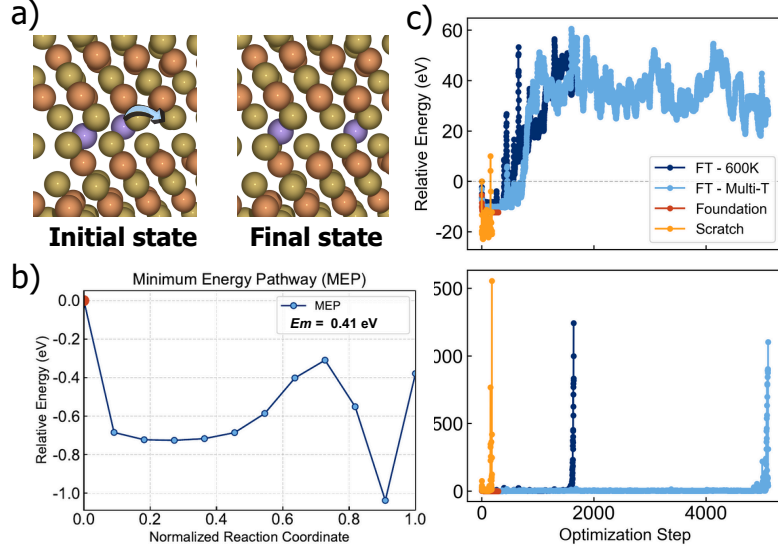


**Fig. 7:** Nudged Elastic Band (NEB) benchmark of MACE models for a Cr atom migration. (a) Visualization of the initial and final states of the diffusion pathway. (b) The converged Minimum Energy Pathway (MEP) calculated with the MACE foundation model, yielding a migration barrier of 0.41 eV. (c) The evolution of the relative system energy (top panel) and the maximum force ( $f_{max}$ , bottom panel) during the NEB optimization for each model. The foundation model (red) converges smoothly. In contrast, the scratch (orange), FT-600K (dark blue), and FT-MultiT (light blue) models all exhibit explosive behavior, where a rapid increase in  $f_{max}$  indicates instability and leads to the termination of the calculation.